Environmental Science and Pollution Research (2024) 31:6835–6846
https://doi.org/10.1007/s11356-023-31567-5

RESEARCH ARTICLE

Efficient removal of organic pollutants by activation of peroxydisulfate with the magnetic $CoFe_2O_4$/carbon nanotube composite

Yawei Shi[1] · Yi Zhang[1] · Guobin Song[1] · Ya Sun[1] · Guanghui Ding[1]

Received: 15 October 2023 / Accepted: 11 December 2023 / Published online: 28 December 2023
© The Author(s), under exclusive licence to Springer-Verlag GmbH Germany, part of Springer Nature 2023

Abstract

A magnetic composite of $CoFe_2O_4$ and carbon nanotube (CNT) was prepared using the solvothermal approach and then employed for the activation of peroxydisulfate (PDS) to degrade reactive black 5 (RB5) and other organic pollutants. Characterization results of the composite catalyst revealed the successful loading of spherical $CoFe_2O_4$ particles on CNTs, possessing abundant porosity as well as magnetic separation capability. Under the degradation conditions of 0.2 g/L $CoFe_2O_4$-CNT dosage and 4 mM PDS dosage, the removal efficiencies of 10 mg/L RB5 and other pollutants were in the range of 94.5 to ~ 100%. The effects of pH, co-existing ions/humic acid, and water matrices as well as the reusability of the catalyst were also investigated in detail. Furthermore, the degradation mechanism and pathway were proposed based on quenching experiments, LC–MS analysis, and density functional theory (DFT) calculations, and the toxicity of the degradation products was evaluated in the quantitative structure–activity relationship approach.

Keywords $CoFe_2O_4$ · Orbital-weighted Fukui function · Organic pollutants · Peroxydisulfate · Toxicity evaluation

Introduction

The presence of various organic pollutants in the water environmental poses significant threats to human health and the survival of various organisms, causing severe harm to the ecological environment. Currently, several technologies have been adopted for treating organic pollutants in water, including adsorption, membrane separation, and the advanced oxidation process (Collivignarelli et al. 2019; Shi et al. 2022a). Among these, the advanced oxidation process has gained widespread use in wastewater treatment due to its high removal efficiency towards various organic pollutants. Recently, persulfate-based advanced oxidation is receiving increasing attention. In this approach, the $SO_4^{\cdot-}$ radical is generated through the activation of peroxymonosulfate (PMS) or peroxydisulfate (PDS) (Kohantorabi et al. 2021). The redox potential of $SO_4^{\cdot-}$ in the range of 2.5–3.1 V (Zhang et al. 2021) is close to that of the ·OH radical produced in other advanced oxidation processes such as Fenton, photocatalytic and ozone oxidation. Notably, $SO_4^{\cdot-}$ is more stable than ·OH and can function effectively across a wide pH range (Giannakis et al. 2021). Consequently, persulfate-based advanced oxidation has been extensively investigated to degrade a variety of organic pollutants in water including dyes, antibiotics, endocrine disruptors, and others (Sarkar et al. 2022).

In comparison to PMS, PDS in the form of potassium or sodium salts is considered to be more stable and cost-effective (Li et al. 2021). However, PDS exhibits slow self-decomposition rates to produce active radicals. Consequently, activation methods are typically employed to enhance its reactivity towards the oxidation of organic pollutants. Thermal (Ren et al. 2021), ultraviolet (Tian et al. 2022), ultrasound (Monteagudo et al. 2018), and electrochemical (Araújo et al. 2022) activation approaches have been studied, where the introduction of external energy in different forms boosted the activation of PDS and the generation of active species. Another approach relies on the employment of catalysts, including homogenous and heterogeneous ones. Although homogenous catalysts, usually transition metal ions, such as Fe^{2+}, Co^{2+}, Ag^{+}, etc., are easy to handle and highly efficient, the remaining metal ions in treated water may pose additional risks. Considering this,

Responsible Editor: Guilherme Luiz Dotto

✉ Guanghui Ding
guanghuiding@dlmu.edu.cn

[1] College of Environmental Science and Engineering, Dalian Maritime University, Dalian 116026, China

heterogeneous catalysts are more welcome from an environmental viewpoint.

Carbon materials as a large group of heterogeneous catalysts have been regarded as promising candidates for persulfate activation. Different types of carbon materials have been investigated, and carbon nanotubes (CNTs) stand out due to their large surface areas and strong stabilities (Apul and Karanfil 2015). Although CNTs showed outstanding performance in the activation of persulfate, the separation of them after the degradation of organic pollutants remains a challenging issue. In our previous work, magnetic Fe_3O_4 particles were combined with CNTs by a facile one-pot solvothermal method to form a magnetic Fe_3O_4-CNT composite, which was then employed for PDS activation towards the degradation of several organic pollutants (Shi et al. 2022b). However, Fe_3O_4 only benefited magnetic separation and was found to show limited catalytic effect in that reaction system (Shi et al. 2022b), which was probably attributed to the relatively low reactivity of iron species. As an alternative, Co_3O_4 also possesses magnetic property and has been proved to be an efficient catalyst for persulfate activation (Peng et al. 2022; Qin et al. 2022). However, compared to iron species, cobalt species are more toxic. When using single Co_3O_4 as the catalyst, the leached high concentration of cobalt ions may form secondary pollution. In our another previous work (Wang et al. 2022b), Bi_2O_3 was introduced in combination with Co_3O_4 to reduce the leaching of cobalt. Nevertheless, Bi_2O_3 shows no magnetic property and the Co_3O_4-Bi_2O_3 catalyst is not suitable for magnetic separation. In comparison with Co_3O_4-Bi_2O_3, the spinel catalyst of $CoFe_2O_4$ may be more applicable, which is also magnetic and has a better resistance to cobalt leaching thanks to its strong Co–Fe interactions (Wang et al. 2020).

Based on these previous works, we further prepared a $CoFe_2O_4$-CNT composite using the same one-pot solvothermal method by replacing the single iron salt precursor with mixed precursors of both iron and cobalt salts. The $CoFe_2O_4$-CNT/PDS system was then investigated for PDS activation towards the degradation of reactive black 5 (RB5) and other organic pollutants. The effects of various operational and environmental factors have been studied, as well as the reaction mechanism, the degradation pathway, and toxicity evaluation of degradation products.

Experimental

Material and characterization

Multi-walled CNTs with outer diameters of 4–6 nm, lengths of 10–20 μm, and purity over 98% were purchased from Chengdu Organic Chemical Co., Ltd. $CoFe_2O_4$-CNT was fabricated in a one-pot solvothermal method similar to the one reported in our previous work when preparing Fe_3O_4-CNT (Shi et al. 2022b), except that a mixture of $FeCl_3{\cdot}6H_2O$ and $Co(NO_3)_2{\cdot}6H_2O$ (molar ratio of Fe/Co = 2:1) was added instead of single $FeCl_3{\cdot}6H_2O$. A series of methods have been conducted to characterize the composite $CoFe_2O_4$-CNT catalyst, including scanning electron microscope (SEM), X-ray diffraction (XRD), nitrogen sorption, X-ray photoelectron spectroscopy (XPS), vibrating sample magnetometer (VSM), and zeta potential analysis. Inductively coupled plasma-mass spectrometry (ICP-MS), open circuit potential (OCP) test, and liquid chromatography-mass spectrometer (LC–MS) analysis were also employed when investigating the degradation mechanism and pathway. More details for the reagents and characterization methods have been provided in Text S1 in Supplementary Materials.

Catalytic oxidation experiments

For the catalytic degradation experiments, appropriate amounts of the $CoFe_2O_4$-CNT catalyst and PDS were introduced into a 250-mL three-necked flask containing 100 mL of pollutant solution prepared in advance. The flask was immersed in a water bath connected to a mechanical stirring apparatus set at 500 r/min. The concentration of the pollutants was determined using a UV–visible spectrophotometer (TU-1901, Beijing Puxi, China). More details for the catalytic oxidation experiments have been provided in Text S2 in Supplementary Materials.

Theoretical calculation and toxicity evaluation

The density functional theory (DFT) calculations were conducted with Gaussian 16 program (Frisch et al. 2016) and the Multiwfn software (Lu and Chen 2012). The results were then visualized with the Virtual Molecular Dynamic (VMD) software (Humphrey et al. 1996). The Ecological Structure Activity Relationships (ECOSAR, v2.2) software was used for toxicity evaluation. More details have been provided in Text S3 in Supplementary Materials.

Results and discussion

Characterization of the catalyst

SEM analysis was first used to characterize the morphology of the $CoFe_2O_4$-CNT composite catalyst. As shown in Fig. 1 a and b, aggregates of $CoFe_2O_4$ particles possessed a spherical morphology, which were dispersed with the CNT branches. XRD was then used to characterize the crystal structure of the catalyst, which revealed distinct diffraction peaks at various 2θ values (Fig. 1c). Most of the peaks were

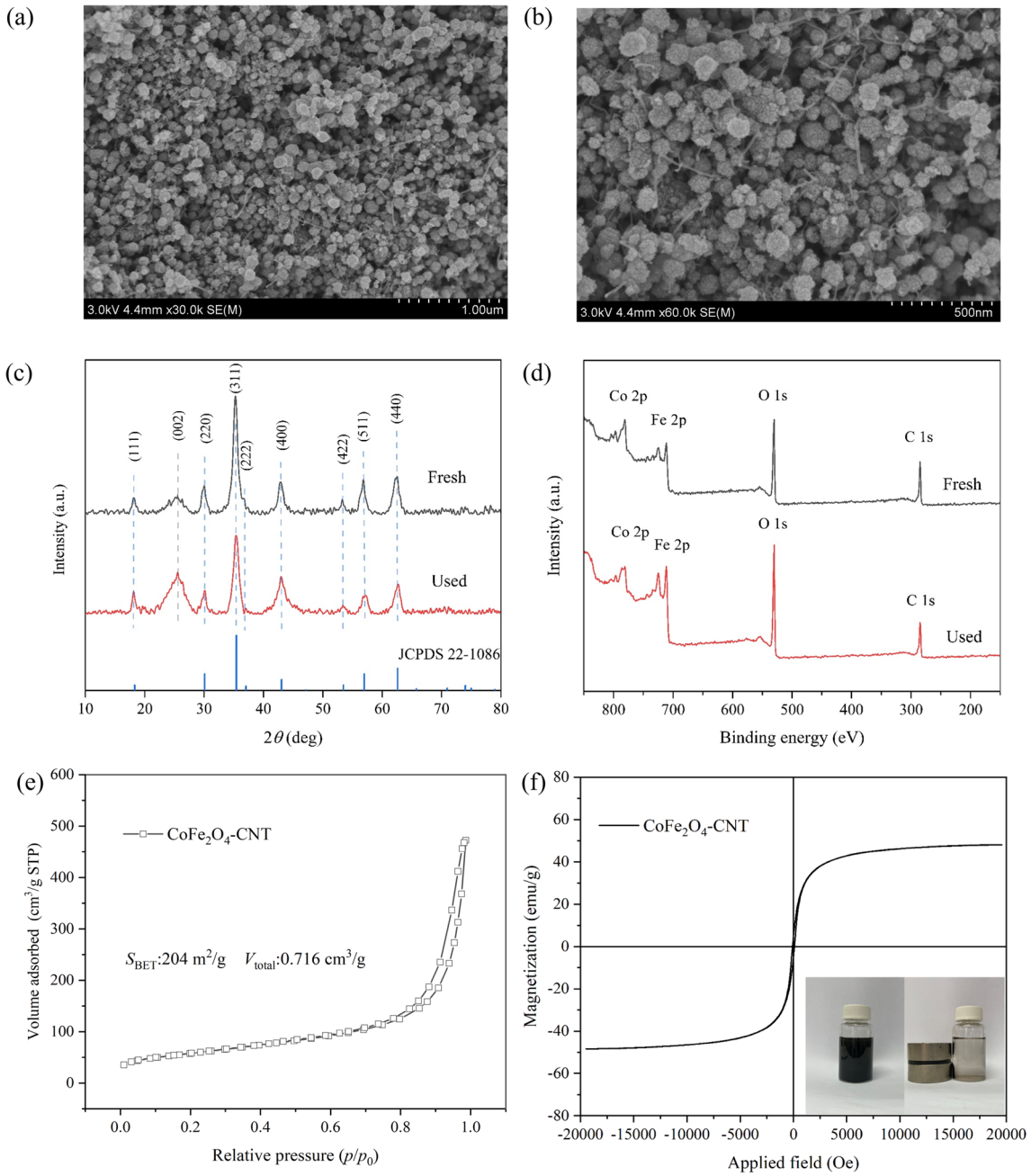

Fig. 1 SEM images (**a**, **b**), XRD patterns (**c**), XPS spectra (**d**), nitrogen sorption isotherm (**e**), and magnetization curve (**f**) of the $CoFe_2O_4$-CNT catalyst

in accordance with the standard pattern of $CoFe_2O_4$ (JCPDS 22–1086) except for the broad band at around 26°, which was ascribed to the (002) crystal plane of CNT (Yang et al. 2023). This again verified the co-existence of $CoFe_2O_4$ and CNT in the composite catalyst, in consistent with the SEM results. To further investigate the chemical structure of the composite, XPS analysis was performed. As illustrated in Fig. 1d, the peaks of C 1 s, O 1 s, Fe 2p, and Co 2p could be clearly observed as expected. Furthermore, deconvolution of the Fe 2p and Co 2p peaks was conducted and the results were summarized in Figure S1 and Table S1-S2. In the Fe 2p spectrum (Figure S1a), the two binding energies at around 726.0 and 713.5 eV were attributed to Fe(III) in tetrahedral sites (A-sites) in the spinel-type $CoFe_2O_4$, while the two at 724.1 and 710.9 eV were assigned to Fe(III) in octahedral sites (B-sites) (Wang et al. 2012; Zou et al. 2021). Similarly, for the Co 2p spectrum (Figure S1b), the two binding energies at 797.5 and 782.3 eV, and the other two at 796.3

and 780.6 eV, indicated the presence of Co(II) in tetrahedral (A-sites) and octahedral sites (B-sites), respectively (Wang et al. 2012; Zou et al. 2021).

Adsorption of the reactants is important for the catalytic oxidation process with the $CoFe_2O_4$-CNT/PDS system. On the one hand, activation of PDS molecules took place on the surface of the $CoFe_2O_4$-CNT catalyst after they were adsorbed. On the other hand, the produced reactive oxidative species (ROSs) usually possessed short lifetimes, and it is more favorable to oxidize the adsorbed pollutants because they were closer in space. Generally, a large specific surface area and abundant porosity indicated that there was more space on the catalyst surface for the adsorption of the reactants. Thus, nitrogen sorption test was used to characterize porosity of the catalyst. According to the nitrogen sorption isotherm (Fig. 1e), the composite possessed a large specific area (S_{BET}) of 204 m^2/g and abundant porosity with a pore volume (V_t) of 0.716 cm^2/g, which were favorable for the adsorption of the reactants and the subsequent catalytic oxidation reaction. In addition, the catalyst showed a saturation magnetization of 48.0 emu/g as revealed by VSM analysis (Fig. 1f). When other conditions are identical, a larger saturation magnetization means that it is easier to separate the catalyst magnetically. The large saturation magnetization of the $CoFe_2O_4$-CNT catalyst indicated that it could be facially magnetically separated, and this was further confirmed in Fig. 1f inset, which showed that the catalyst could be facially separated with an external magnet.

Catalytic oxidation performance of organic pollutants

Using the $CoFe_2O_4$-CNT/PDS system, the catalytic oxidation performances of RB5 and other organic pollutants were studied. The effects of several operation factors have been investigated, including dosage of $CoFe_2O_4$-CNT, dosage of PDS, initial concentration of RB5, initial pH, and reaction temperature (Fig. 2). The corresponding kinetic fitting results and k_{obs} values are shown in Figure S2 in Supplementary Materials. As illustrated in Fig. 2a, RB5 removal was 20.4% in the presence of PDS only, which was attributed to the direct oxidation of RB5 by PDS. With the addition of 0.1 g/L $CoFe_2O_4$-CNT, RB5 removal was significantly increased to 80.4%, indicating the high catalytic efficiency of the catalyst. An increased dosage of 0.2 g/L provided more active sites, leading to a further increase in RB5 removal to 96.8%. However, further increasing the dosage to 0.3 g/L did not result in obvious improvement in RB5 removal. From a practical viewpoint, the dosage of 0.2 g/L was selected to decrease the catalyst cost. At this catalyst dosage, the effect of PDS dosage was further investigated (Fig. 2b). In the absence of PDS, RB5 removal was found to be 44.4%. This high removal by adsorption was attributed to the abundant porosity of the catalyst, which was verified above in Fig. 1e. Note that the sum of RB5 removals with catalyst only (44.4%) and with PDS only (20.4%) was 64.8%, which was much lower than the removal obtained in the presence of both (96.8%). This clearly proved the high catalytic efficiency of the $CoFe_2O_4$-CNT/PDS system. With an increase in the PDS dosage, RB5 removal was enhanced first and reached a maximum at 4 mM. Nevertheless, at a higher dosage of 5 mM, excessive PDS resulted in decreased RB5 removal, which was probably due to self-quenching reactions occurred between PDS and the produced active species (Maifadi et al. 2022). Therefore, the dosage of PDS was selected as 4 mM. The effect of initial RB5 concentration was investigated in the range of 5–40 mg/L. As shown in Fig. 2c, as the initial RB5 concentration increases, its removal gradually decreases. This is because when the amounts of catalyst and oxidant remain constant, the catalytic system can provide limited active sites and reactive species. At a higher initial RB5 concentration, there will be more RB5 and more oxidation intermediates in the system, leading to more fierce competition and resulting in a decrease in the removal efficiency. However, even at a RB5 concentration of 40 mg/L, a high removal of 81.6% could be achieved, indicating the high catalytic performance of the $CoFe_2O_4$-CNT/PDS system. Although decreasing the initial concentration led to enhanced removal efficiency, dilution led to the consumption of more oxidant and catalyst at a fixed mass of pollutant. Therefore, to make a compromise, the initial concentration was selected as 10 mg/L to achieve a moderate removal efficiency.

The influence of initial pH was depicted in Fig. 2d. The removal of RB5 was above 90% in the initial pH range of 3–9, but it declined to 82.1% at a higher pH value of 11. The highest removal efficiency of 97.7% was obtained at pH 3. From a practical viewpoint, additional acid is required to tailor the solution pH, leading to increased cost. At the spontaneous pH of the RB5 solution (around 6.7), the removal efficiency was 96.8%, which was only slightly lower than the value at pH 3. Therefore, the initial pH was not tailored for subsequent experiments. The decreased removal efficiency under alkaline conditions may be attributed to several reasons. As revealed by zeta potential measurements (Figure S3), the surface of the $CoFe_2O_4$-CNT catalyst surface carries negative charges under alkaline conditions. On the one hand, this will lead to enhanced electrostatic repulsion between the anionic RB5 and the catalyst surface, inhibiting its adsorption and degradation. On the other hand, this will also hinder the adsorption and subsequently activation of the PDS oxidant, which is also a negatively charged species in the form of $S_2O_8^{2-}$. In addition, the large amount of OH^- under alkaline conditions may react with surface metal species to form iron hydroxide complexes, suppressing the catalytic performance of the catalyst (Xu et al. 2019).

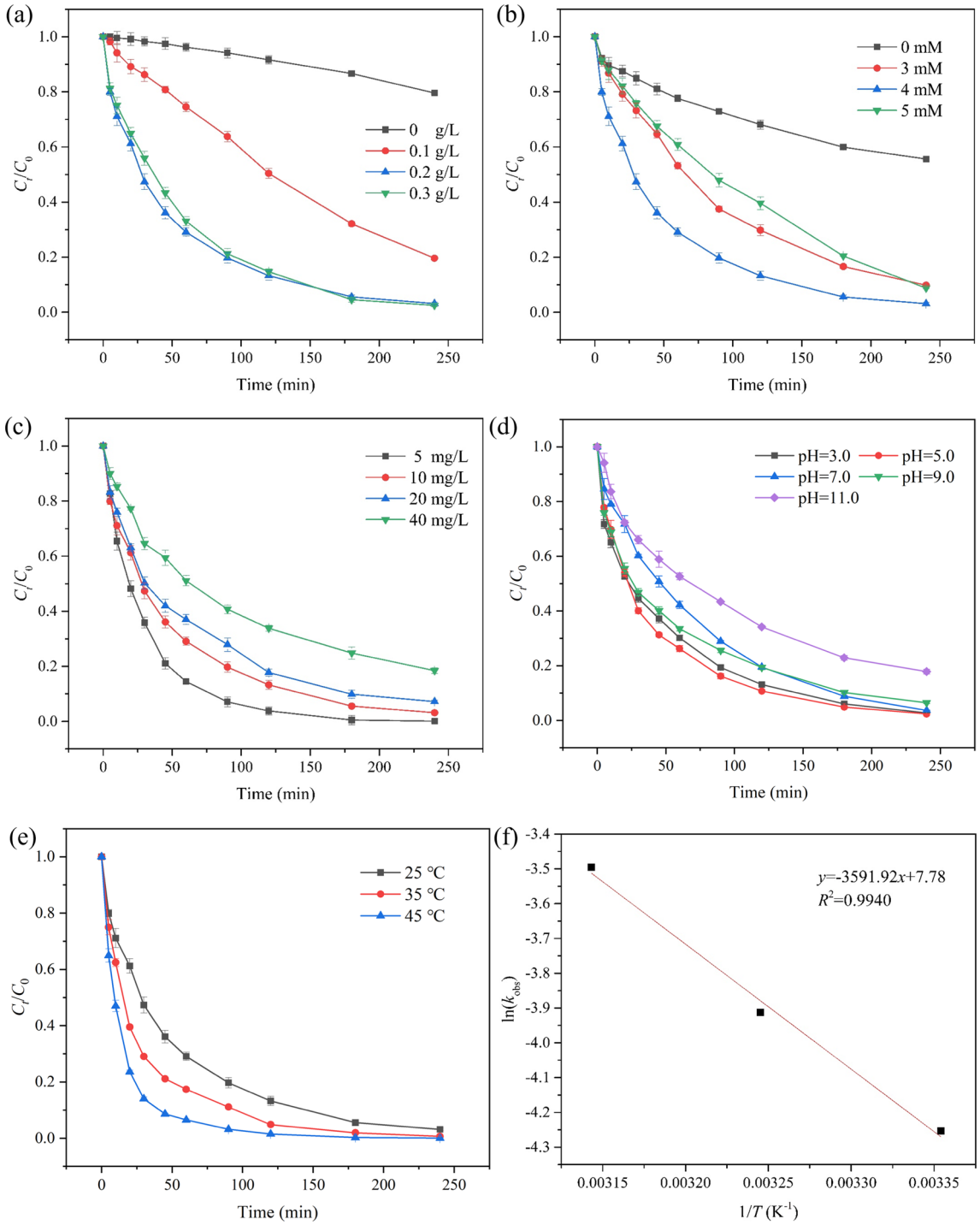

Fig. 2 Effects of $CoFe_2O_4$-CNT dosage (**a**), PDS dosage (**b**), initial concentration of RB5 (**c**), initial pH (**d**), temperature (**e**), and linear fitting in the Arrhenius model (**f**) Experimental conditions unless otherwise stated: $CoFe_2O_4$-CNT dosage = 0.2 g/L, PDS dosage = 4 mM, initial RB5 concentration = 10 mg/L, no pH adjustment, temperature = 25 ℃

Finally, the impact of reaction temperature on the removal of RB5 was studied. As revealed in Fig. 2e, RB5 removal was improved from 96.8 to ~ 100% from 25 to 45 ℃, and k_{obs} increased sharply from 0.0142 to 0.0304/min. Based on the Arrhenius equation, the activation energy (E_a) was calculated to be 29.9 kJ/mol (Fig. 2f), which was a relatively low value and again indicated the high catalytic performance of the reaction system (Ma et al. 2020). Additional heat is required to maintain a higher temperature, leading to increased cost. Therefore, the temperature

was selected to be 25 ℃, which was the ambient room temperature.

In summary, for the selection of specific operation conditions, both the goal of a higher removal efficiency and the economy of the treatment process are considered. The selected conditions were as follows: $CoFe_2O_4$-CNT dosage = 0.2 g/L, PDS dosage = 4 mM, initial RB5 concentration = 10 mg/L, no pH adjustment, temperature = 25 ℃.

Inorganic ions and natural organic matter widely presented in real water matrices may impact the degradation performance. Considering this, their effects were investigated furthermore. When Cl^- and $H_2PO_4^-$ were added, the removal efficiencies of RB5 decreased from 96.8 to 95.7% and 94.9% (Fig. 3a), and the corresponding k_{obs} dropped from 0.0142 to 0.0129 and 0.0125/min, respectively (Figure S4a). The added Cl^- and $H_2PO_4^-$ could react with the active species such as ·OH and $\cdot SO_4^{\cdot -}$ radicals generated in the catalytic system, forming weaker radicals and thus slightly inhibiting the degradation process (Fu et al. 2019; Shi et al. 2020). Compared to Cl^- and $H_2PO_4^-$, the addition of HCO_3^- and HPO_4^{2-} could not only react with active radicals to form less reactive ones but also lead to an increase in the initial pH of the solution. As a result, they exerted more significant suppression effects, resulting in decreased RB5 removal to 94.5% and 91.3% (Fig. 3a) as well as decreased k_{obs} to 0.0118 and 0.0099/min (Figure S4a). The impact of HA was limited compared to these inorganic ions, leading to a similar removal efficiency of 96.4% and a similar k_{obs} of 0.0141/min.

When investigating the performance of the $CoFe_2O_4$-CNT/PDS system above, deionized water was used and RB5 was employed as the target pollutant. For practical application of the catalyst, different water matrices and various pollutants may be faced with. To address this issue, the performance of the catalytic system was further evaluated in several water matrices including tap water, lake water and sea water. In these different matrices, RB5 removal efficiencies all remained above 95% (Fig. 3b) although the k_{obs} values decreased to some extent (Figure S4c), which could be ascribed to the inorganic ions and organic matters

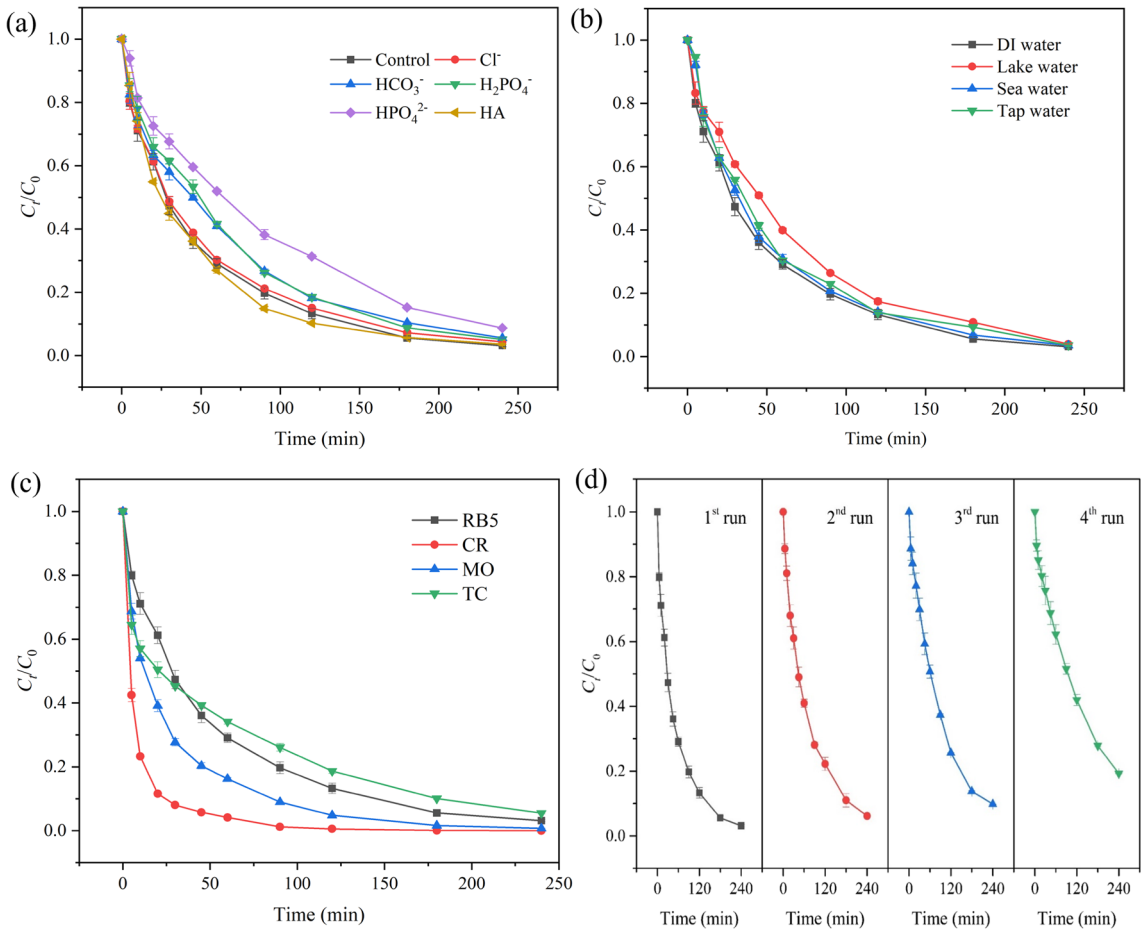

Fig. 3 Effects of anions and HA (**a**), water matrices (**b**), and pollutant type (**c**) on the degradation performance and reusability of the $CoFe_2O_4$-CNT catalyst (**d**). Experimental conditions: $CoFe_2O_4$-CNT dosage = 0.2 g/L, PDS dosage = 4 mM, initial pollutant concentration = 10 mg/L, no pH adjustment, temperature = 25 ℃

in them as well as higher pH values of them (Table S3). This indicated the potential of this reaction system for utilization in real water matrices. After that, several other organic pollutants were tested as the target, including another two dye pollutants (Congo red (CR) and methyl orange (MO)) and an antibiotic pollutant (tetracycline, TC). As depicted in Fig. 3c, these organic pollutants with different structures could be efficiently removed, achieving high removal efficiencies of ~ 100%, 99.3%, and 94.5%, respectively. These results showed that the $CoFe_2O_4$-CNT/PDS system is applicable to various water matrices and various organic pollutants, suggesting its wide practical applicability.

Finally, reusability of the $CoFe_2O_4$-CNT catalyst was evaluated. The RB5 removal efficiencies were 96.8%, 93.8%, 90.2% and 80.7% in four consecutive catalytic runs (Fig. 3d). Metal leaching may be a possible reason for catalytic deactivation. According to ICP results, the amounts of leached Fe and Co were 0.38 and 1.30 mg/L, respectively. Based on this result, an additional degradation experiment was conducted by adding a homogenous mixture of Fe^{2+} and Co^{2+} instead of the heterogenous $CoFe_2O_4$-CNT catalyst. The result showed that compared to the case of single PDS (20.4%), the Fe^{2+}/Co^{2+}/PDS system only slightly promoted RB5 removal (29.7%) (Figure S5). In addition, the XRD pattern of used $CoFe_2O_4$-CNT was similar to that of the fresh one (Fig. 1c), indicating the structural stability of the catalyst. Therefore, the main reason for the deactivation of $CoFe_2O_4$-CNT was ascribed to the accumulation of residue degradation products on the catalyst surface, which occupied the active sites and inhibited the adsorption and subsequently oxidation of organic pollutants (Wang et al. 2022a, b).

Reaction mechanism

In PDS-based catalytic oxidation processes, several ROSs may be involved, including ·OH, $SO_4{\cdot}^-$, $O_2{\cdot}^-$, $^1O_2$, and high-valent metal-oxo species. To investigate their contributions in the $CoFe_2O_4$-CNT/PDS system, several quenchers were added, including MeOH, PMSO, FFA, and BQ. MeOH can efficiently quench both ·OH and $SO_4{\cdot}^-$ (Wang et al. 2023), while PMSO is a quencher for high-valent metal-oxo species (Chi et al. 2021; Feng et al. 2021). FFA and BQ are known as quenchers for $^1O_2$ (Guo et al. 2021) and $O_2{\cdot}^-$ (Yang et al. 2021), respectively. As illustrated in Fig. 4a and Figure S6a, all the four quenchers led to declined RB5 removal and k_{obs} value, indicating the contributions of all these reactive species in the catalytic oxidation process. To gain further insights into the contributions of these species, the four quenchers were simultaneously introduced into the system. This led to a significant decrease in RB5 removal, reducing it to 42.1% (Fig. 4b). This value approached the removal efficiency of 44.4% when only the catalyst was present, and the obtained k_{obs} values were also close to each other in these two cases (Figure S6b). This indicated the near-complete inhibition of the catalytic reaction, ruling out the involvement of other reaction mechanisms.

It should be noted that the reaction mechanism in this $CoFe_2O_4$-CNT/PDS system was different from the Fe_3O_4-CNT/PDS system in our previous work, where the non-radical surface-mediated electron-transfer mechanism played an indispensable role (Shi et al. 2022b). In the current work, in-situ OCP test was conducted as well. Nevertheless, although the potential of the $CoFe_2O_4$-CNT catalyst was increased with the addition of PDS, the subsequent addition of RB5 did not result in a potential drop (Figure S7). This phenomenon was inconsistent with the result in the Fe_3O_4-CNT/PDS system where an apparent drop was observed (Shi et al. 2022b). Thus, the contribution of non-radical surface-mediated electron-transfer mechanism was ruled out.

XPS measurements further revealed the divergent reaction mechanisms. As discussed in the "Characterization of the catalyst" section, Fe and Co elements in the catalyst existed in form of Fe(III) and Co(II). After the catalytic run, the Fe 2p spectrum of the used catalyst was similar with that of the fresh one, showing the same number of deconvoluted peaks at close binding energies (Figure S8a and Table S1). In contrast, two additional peaks appeared

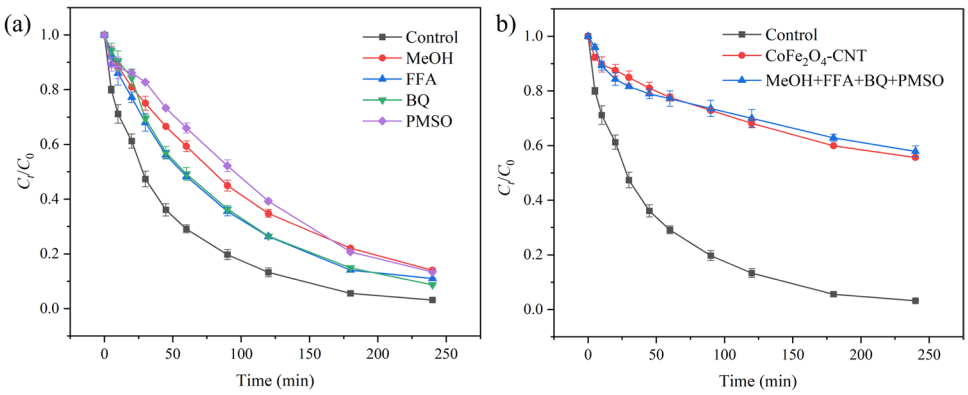

Fig. 4 Effects of single quencher (**a**) and multiple quenchers (**b**) on RB5 degradation in the $CoFe_2O_4$-CNT/PDS system

at 792.7 and 780.0 eV in the Co 2p spectrum of the used catalyst, which could be ascribed to Co(III) species (Figure S8b and Table S1) (Zou et al. 2021). Based on this result, Fe(III) species did not take part in the catalytic process but Co(II) did, which activated PDS and was partly transformed into Co(III). Although Co(III) can also activate PDS to form reactive species, the transformation from Co(III) to Co(II) is much slower than the transformation from Co(II) to Co(III) (Liu et al. 2021b). As a result, an increase in the Co(III) fraction was observed for the used catalyst. Again, this was inconsistent with the Fe_3O_4-CNT/PDS system, where it was found that Fe_3O_4 only played a role in magnetic separation and made little contribution to the activation of PDS (Shi et al. 2022b).

Degradation pathway and toxicity evaluation

To scrutinize the oxidation products generated in the degradation process of RB5, LC–MS analysis has been conducted on the treated RB5 solution. To assist the analysis, DFT calculations have been performed to obtain the orbital-weighted Fukui functions (f_{OW}^- and f_{OW}^0) of RB5 (Fig. 5). The condensed Fukui indexes were summarized in Table S4. According to previous reports (Deng et al. 2021), f_{OW}^- and f_{OW}^0 represent the tendency of different sites in the molecule towards radical attack and electrophilic attack. The larger the values, the more susceptible the sites. Based on Fig. 5 and Table S4, O12-14, O16-18, N19-20, and N37-38 sites exhibited higher susceptibility in the oxidative degradation process.

Combining the DFT calculation results above and the LC–MS results (Figure S9), the plausible degradation pathway of RB5 in the $CoFe_2O_4$-CNT/PDS system has been proposed (Fig. 6). The attack on O12-14 and O16-18 sites of compound A (the target pollutant of RB5) results in the formation of compound B. Subsequently, the N19 and N20 sites of compound B undergo cleavage, giving rise to the generation of compound D and compound E. The N20 site in compound D is attacked, leading to the production of compound G, which is subsequently subjected to desulfurization to yield compound J. Meanwhile, the N37 and N38 sites in compound E are susceptible to attack, culminating in the formation of compound H, which is further protonated to yield compound K (Hisaindee et al. 2013). Additionally, the N19 and N38 sites of compound A are subject to attack, leading to the formation of compound C and compound D. Subsequently, the N37 site in compound C is targeted for attack, resulting in the creation of compound F. Compound F further engages in an attack on the O12-14 and O16-18 sites, ultimately producing compound I (Liu et al. 2021a).

Moreover, predictions regarding the potential toxicological effects of these oxidation products have been conducted. As shown in Fig. 7, RB5 (designated as compound A) and its oxidation products (designated as compounds B-K) exhibited varying degrees of acute and chronic toxicity towards three indicator species. Compound G exhibited higher acute and chronic toxicity values for the three indicator species, indicating a decrease in both acute and chronic toxicity compared to RB5. Compound J has higher toxicity values for daphnia and fish (Fig. 7c, d, f), indicating that its toxicity to daphnia and chronic toxicity to fish are reduced compared

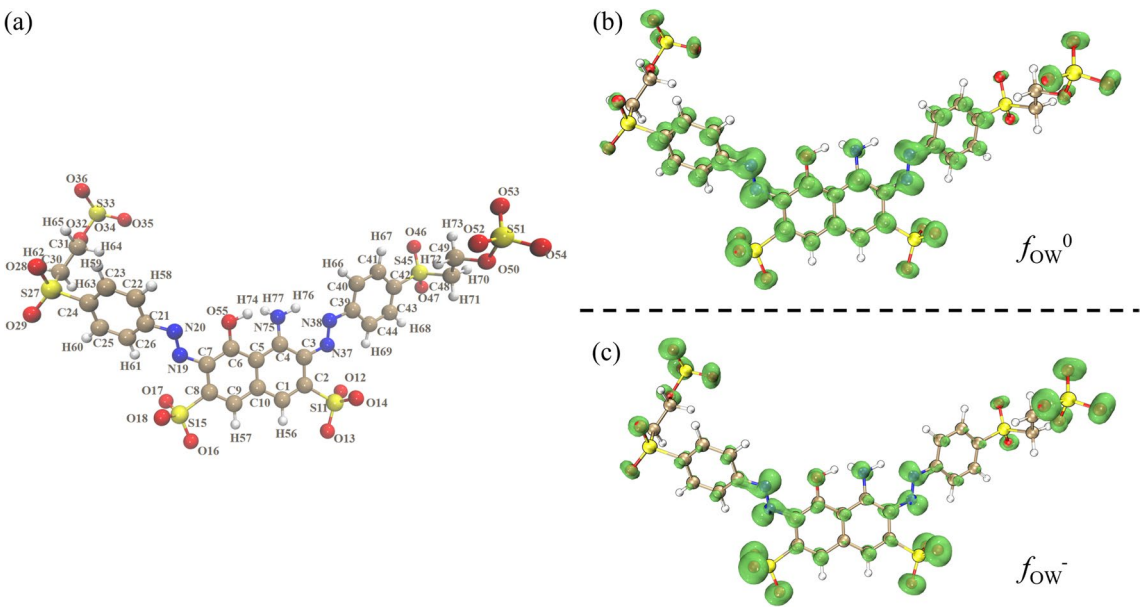

Fig. 5 The optimized molecular structure of RB5 (**a**) and the orbital-weighted Fukui functions of f_{OW}^0 (**b**) and f_{OW}^- (**c**)

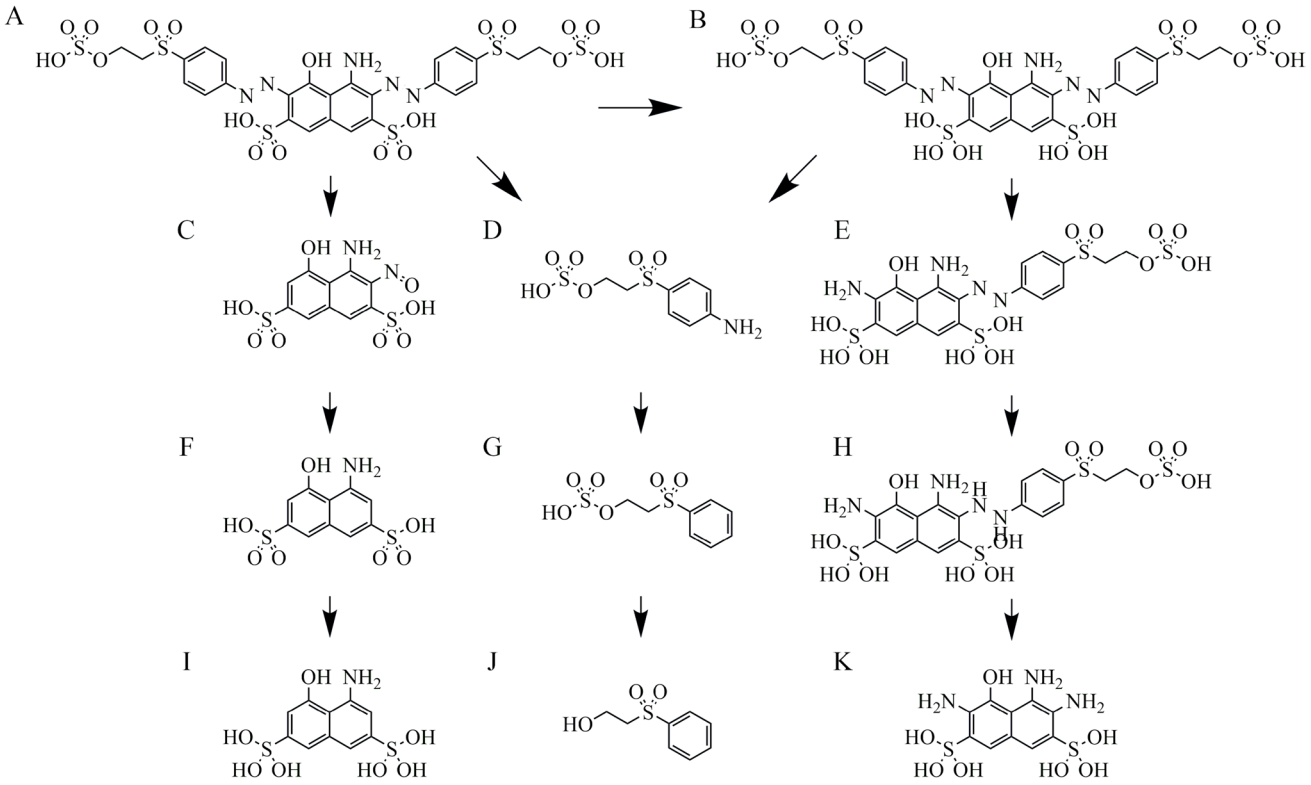

Fig. 6 The plausible degradation pathway of RB5

to RB5. For other products, the EC50 and ChV values are relatively lower, indicating increased toxicity compared to RB5. In addition, the orders of acute and chronic toxicity of these products for the same species are different. For example, for daphnia, compound D ranks eighth in terms of acute toxicity among all products (Fig. 7c) and is considered non-toxic (LC50 > 10 mg/L), but its chronic toxicity ranks fifth (Fig. 7d) and is considered toxic (ChV > 10 mg/L) (Zhu et al. 2021). Therefore, when conducting toxicity prediction, both acute and chronic toxicity should be considered to draw a comprehensive conclusion. For different species, the toxicity trends of most products are similar except for compound C and D. These two compounds are relatively safe for green algae and fish, but have significant chronic toxicity for daphnia (Fig. 7d). In general, toxicity prediction indicated that some oxidation products with stronger toxicity than RB5 are obtained after treated with the $CoFe_2O_4$-CNT/PDS system. Therefore, from a practical perspective, further remediation technologies such as adsorption and membrane separation may be required to remove these residual toxic products.

Based on the findings above, more research is needed in future works before using the $CoFe_2O_4$-CNT/PDS system for practical water treatment. On the one hand, although the $CoFe_2O_4$-CNT/PDS system showed high performance for the removal of several single organic pollutant, different organic pollutants may co-exist for real water treatment. According to the results in Fig. 3c, different removal efficiencies were obtained for different pollutants although their concentrations were the same. Therefore, the selectivity and the overall removal efficiency for mixed pollutants should be investigated. On the other hand, based on the toxicity evaluation results in Fig. 7, some of the oxidation products showed decreased toxicity compared to the parent RB5 while some others showed increased toxicity. Since these products were in different concentrations in the treated water, the overall toxicity of the treated water remained unknown. In future works, it is suggested to conduct some toxicity evaluation experiments using some indicator species to provide a better understanding of the change in toxicity after being treated with the $CoFe_2O_4$-CNT/PDS system.

Conclusion

The composite of $CoFe_2O_4$-CNT was synthesized in a facile solvothermal approach, serving as a catalyst in activation of PDS towards the degradation of RB5 and other organic pollutants. SEM, XRD, and XPS measurements verified the successfully preparation of the composite catalyst. In addition, nitrogen-sorption and VSM results showed that the catalyst possessed a large surface area of 204 m^2/g and a saturation magnetization of 48.0 emu/g. When employed

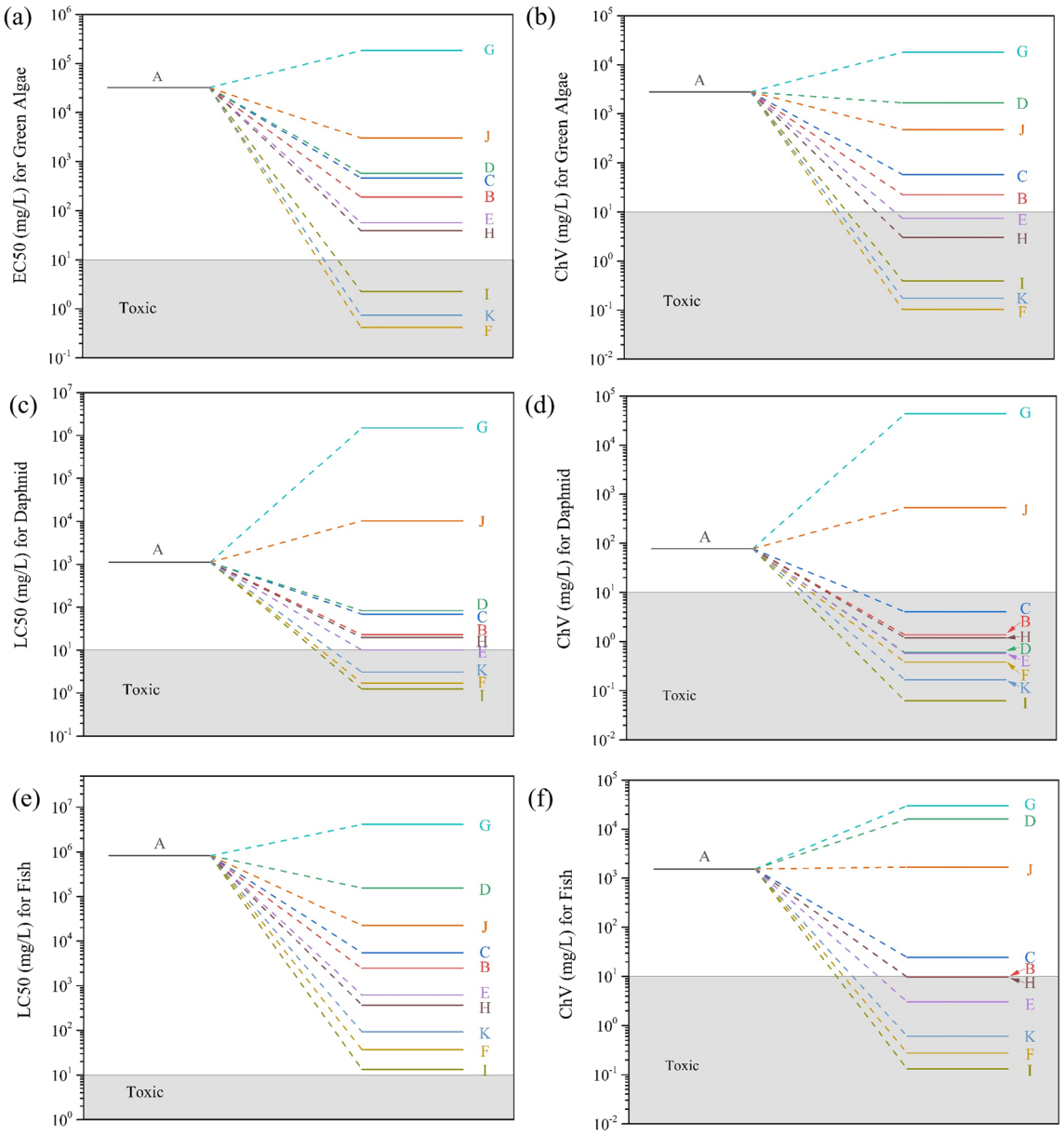

Fig. 7 Acute (**a**, **c**, **e**) and chronic toxicity (**b**, **d**, **f**) of RB5 and its degradation products for green algae, daphnia, and fish

in combination with PDS for pollutant degradation, the effects of various operational conditions have been investigated. Under the experimental conditions of 0.2 g/L $CoFe_2O_4$-CNT, 4 mM PDS, initial pollutant concentration of 10 mg/L and temperature of 25 ℃, the removal efficiencies of several organic pollutants including RB5, CR, MO, and TC were in the range of 94.5 to ~ 100%. The effects of pH, co-existing inorganic salts and HA as well as water matrix were also studied, verifying the potential application of the $CoFe_2O_4$-CNT/PDS system for treatment of real water matrices. Based on quenching experiments, OCP and XPS analysis, the reaction mechanism in $CoFe_2O_4$-CNT/PDS was found to be different from the Fe_3O_4-CNT/PDS system in our previous work. The additional Co(II) species played an indispensable role in the catalytic oxidation process, which helped to active PDS towards the generation of various reactive oxidation species. Finally, the plausible degradation pathway of RB5 was proposed based on DFT calculations and LC–MS analysis, and the toxicity of those degradation products were predicted by ECOSAR using indicator species of green algae, daphnia, and fish.

Supplementary Information The online version contains supplementary material available at https://doi.org/10.1007/s11356-023-31567-5.

Author contribution Yawei Shi: writing—original draft, writing—review and editing, conceptualization. Yi Zhang: methodology, data

curation, investigation. Guobin Song: formal analysis, data curation. Ya Sun: resources. Guanghui Ding: resources, supervision.

Funding This work is financially supported by the Joint Research Fund Liaoning-Shenyang National Laboratory for Materials Science (20180510004), the National Natural Science Foundation of China (51479016, 51908409), and the Fundamental Research Funds for the Central Universities (3132023162).

Data availability All data generated or analyzed during this study are included in this published article (and its supplementary information files).

Declarations

Ethics approval and consent to participate Not applicable.

Consent for publication Not applicable.

Competing interests The authors declare no competing interests.

References

Apul OG, Karanfil T (2015) Adsorption of synthetic organic contaminants by carbon nanotubes: A critical review. Water Res 68:34–55. https://doi.org/10.1016/j.watres.2014.09.032

Araújo KCF, dos Santos EV, Nidheesh PV, Martínez-Huitle CA (2022) Fundamentals and advances on the mechanisms of electrochemical generation of persulfate and sulfate radicals in aqueous medium. Curr Opin Chem Eng 38:100870. https://doi.org/10.1016/j.coche.2022.100870

Chi H, Wan J, Zhou X, Sun J, Yan B (2021) Fe@C activated peroxymonosulfate system for effectively degrading emerging contaminants: analysis of the formation and activation mechanism of Fe coordinately unsaturated metal sites. J Hazard Mater 419:126535. https://doi.org/10.1016/j.jhazmat.2021.126535

Collivignarelli MC, Abba A, Carnevale Miino M, Damiani S (2019) Treatments for color removal from wastewater: state of the art. J Environ Manage 236:727–745. https://doi.org/10.1016/j.jenvman.2018.11.094

Deng J, Ye C, Cai A, Huai L, Zhou S, Dong F, Li X, Ma X (2021) S-doping α-Fe_2O_3 induced efficient electron-hole separation for enhanced persulfate activation toward carbamazepine oxidation: experimental and DFT study. Chem Eng J 420:129863. https://doi.org/10.1016/j.cej.2021.129863

Feng Y, Li Y, Yang B, Yang Z, Fan Y, Shih K, Li H, Wu D, Zhang L (2021) Mechanistic insight into the generation of high-valent iron-oxo species via peroxymonosulfate activation: an experimental and density functional theory study. Chem Eng J 420:130477. https://doi.org/10.1016/j.cej.2021.130477

Frisch MJ, Trucks GW, Schlegel HB, Scuseria GE, Robb MA, Cheeseman JR et al (2016) Gaussian 16 Rev. C.01, Wallingford, CT

Fu H, Zhao P, Xu S, Cheng G, Li Z, Li Y, Li K, Ma S (2019) Fabrication of Fe_3O_4 and graphitized porous biochar composites for activating peroxymonosulfate to degrade p-hydroxybenzoic acid: insights on the mechanism. Chem Eng J 375:121980. https://doi.org/10.1016/j.cej.2019.121980

Giannakis S, Lin K-YA, Ghanbari F (2021) A review of the recent advances on the treatment of industrial wastewaters by sulfate radical-based advanced oxidation processes (SR-AOPs). Chem Eng J 406:127083. https://doi.org/10.1016/j.cej.2020.127083

Guo Y, Yan L, Li X, Yan T, Song W, Hou T, Tong C, Mu J, Xu M (2021) Goethite/biochar-activated peroxymonosulfate enhances tetracycline degradation: Inherent roles of radical and non-radical processes. Sci Total Environ 783:147102. https://doi.org/10.1016/j.scitotenv.2021.147102

Hisaindee S, Meetani MA, Rauf MA (2013) Application of LC-MS to the analysis of advanced oxidation process (AOP) degradation of dye products and reaction mechanisms. TrAC-Trend Anal Chem 49:31–44. https://doi.org/10.1016/j.trac.2013.03.011

Humphrey W, Dalke A, Schulten K (1996) VMD: visual molecular dynamics. J Mol Graph 14:33–38. https://doi.org/10.1016/0263-7855(96)00018-5

Kohantorabi M, Moussavi G, Giannakis S (2021) A review of the innovations in metal- and carbon-based catalysts explored for heterogeneous peroxymonosulfate (PMS) activation, with focus on radical vs. non-radical degradation pathways of organic contaminants. Chem Eng J. 411:127957. https://doi.org/10.1016/j.cej.2020.127957

Li H, Yang Z, Lu S, Su L, Wang C, Huang J, Zhou J, Tang J, Huang M (2021) Nano-porous bimetallic CuCo-MOF-74 with coordinatively unsaturated metal sites for peroxymonosulfate activation to eliminate organic pollutants: Performance and mechanism. Chemosphere 273:129643. https://doi.org/10.1016/j.chemosphere.2021.129643

Liu F, Wang X, Liu Z, Miao F, Xu Y, Zhang H (2021a) Peroxymonosulfate enhanced photocatalytic degradation of Reactive Black 5 by ZnO-GAC: key influencing factors, stability and response surface approach. Sep Purif Technol 279:119754. https://doi.org/10.1016/j.seppur.2021.119754

Liu J, Li Z, Wang M, Jin C, Kang J, Tang Y, Li S (2021b) Eu_2O_3/Co_3O_4 nanosheets for levofloxacin removal via peroxymonosulfate activation: performance, mechanism and degradation pathway. Sep Purif Technol 274:118666. https://doi.org/10.1016/j.seppur.2021.118666

Lu T, Chen F (2012) Multiwfn: a multifunctional wavefunction analyzer. J Comput Chem 33:580–592. https://doi.org/10.1002/jcc.22885

Ma Q, Nengzi L-c, Zhang X, Zhao Z, Cheng X (2020) Enhanced activation of persulfate by AC@$CoFe_2O_4$ nanocomposites for effective removal of lomefloxacin. Sep Purif Technol 233:115978. https://doi.org/10.1016/j.seppur.2019.115978

Maifadi S, Mhlanga SD, Nxumalo EN, Motsa MM, Kuvarega AT (2022) Treatment of salon wastewater by peroxydisulfate based advanced oxidation process (PDS-AOP) under solar light: Synergy through integrated technologies. J Water Process Eng 49:103062. https://doi.org/10.1016/j.jwpe.2022.103062

Monteagudo JM, El-taliawy H, Durán A, Caro G, Bester K (2018) Sono-activated persulfate oxidation of diclofenac: degradation, kinetics, pathway and contribution of the different radicals involved. J Hazard Mater 357:457–465. https://doi.org/10.1016/j.jhazmat.2018.06.031

Peng J, Chang Y, Wang Z, Liu J, Wang S, Zhang Y, Shao S, Liu D, Zhang Y, Shi J, Liu H, Yan G, Cao Z, Gao S (2022) Amlodipine removal via peroxymonosulfate activated by carbon nanotubes/cobalt oxide (CNTs/Co_3O_4) in water. Environ Sci Pollut Res 29:11091–11100. https://doi.org/10.1007/s11356-021-16399-5

Qin Q, Yan L, Liu Z, Liu Y, Gu J, Xu Y (2022) Efficient activation of peroxymonosulfate by nanotubular Co_3O_4 for degradation of Acid Orange 7: performance and mechanism. Environ Sci Pollut Res 29:50135–50146. https://doi.org/10.1007/s11356-022-19434-1

Ren W, Huang X, Wang L, Liu X, Zhou Z, Wang Y, Lin C, He M, Ouyang W (2021) Degradation of simazine by heat-activated peroxydisulfate process: a coherent study on kinetics, radicals and models. Chem Eng J 426:131876. https://doi.org/10.1016/j.cej.2021.131876

Sarkar P, Roy D, Bera B, De S, Neogi S (2022) Enhanced photodegradation of reactive dyes in textile effluent with $CoFe_2O_4$/g-CN heterostructure-mediated peroxymonosulphate activation.

Environ Sci Pollut Res 29:50566–50583. https://doi.org/10.1007/s11356-022-18944-2

Shi Y, Zhu J, Yuan G, Liu G, Wang Q, Sun W, Zhao B, Wang L, Zhang H (2020) Activation of persulfate by EDTA-2K-derived nitrogen-doped porous carbons for organic contaminant removal: radical and non-radical pathways. Chem Eng J 386:124009. https://doi.org/10.1016/j.cej.2019.124009

Shi Y, Chang Q, Zhang T, Song G, Sun Y, Ding G (2022a) A review on selective dye adsorption by different mechanisms. J Environ Chem Eng 10:108639. https://doi.org/10.1016/j.jece.2022.108639

Shi Y, Zhang Y, Song G, Tong L, Sun Y, Ding G (2022b) Efficient degradation of organic pollutants using peroxydisulfate activated by magnetic carbon nanotube. Water Sci Technol 86:2611–2626. https://doi.org/10.2166/wst.2022.371

Tian D, Zhou H, Zhang H, Zhou P, You J, Gang Y, Pan Z, Liu Y, Lai B (2022) Heterogeneous photocatalyst-driven persulfate activation process under visible light irradiation: from basic catalyst design principles to novel enhancement strategies. Chem Eng J 428:131166. https://doi.org/10.1016/j.cej.2021.131166

Wang WP, Yang H, Xian T, Jiang JL (2012) XPS and magnetic properties of $CoFe_2O_4$ nanoparticles synthesized by a polyacrylamide gel route. Mater Trans 53:1586–1589. https://doi.org/10.2320/matertrans.M2012151

Wang Y, Zhang Y, Wang J (2020) Nano spinel $CoFe_2O_4$ deposited diatomite catalytic separation membrane for efficiently cleaning wastewater. J Membrane Sci 615:118559. https://doi.org/10.1016/j.memsci.2020.118559

Wang B, Li S, Wang H, Yao S (2022a) Insight into the performance and mechanism of magnetic $Ni_{0.5}Cu_{0.5}Fe_2O_4$ in activating peroxydisulfate for ciprofloxacin degradation. Water Sci Technol 85:1235–1249. https://doi.org/10.2166/wst.2022.043

Wang L, Wang L, Shi Y, Zhu J, Zhao B, Zhang Z, Ding G, Zhang H (2022b) Fabrication of Co_3O_4-Bi_2O_3-Ti catalytic membrane for efficient degradation of organic pollutants in water by peroxymonosulfate activation. J Colloid Interf Sci 607:451–461. https://doi.org/10.1016/j.jcis.2021.08.086

Wang J, Lv H, Tong X, Ren W, Shen Y, Lu L, Zhang Y (2023) Modulation of radical and nonradical pathways via modified carbon nanotubes toward efficient oxidation of binary pollutants in water. J Hazard Mater 459:132334. https://doi.org/10.1016/j.jhazmat.2023.132334

Xu M, Li J, Yan Y, Zhao X, Yan J, Zhang Y, Lai B, Chen X, Song L (2019) Catalytic degradation of sulfamethoxazole through peroxymonosulfate activated with expanded graphite loaded $CoFe_2O_4$ particles. Chem Eng J 369:403–413. https://doi.org/10.1016/j.cej.2019.03.075

Yang B, Luo Q, Li Q, Meng Y, Lingli L, Liu Y (2021) Selective oxidation and direct decolorization of cationic dyes by persulfate without activation. Water Sci Technol 83:2744–2752. https://doi.org/10.2166/wst.2021.177

Yang F, Hu P, Yang FF, Chen B, Yin F, Hao K, Sun R, Gao L, Sun Z, Wang KJS (2023) CNTs bridged basal-plane-active 2H-MoS_2 nanosheets for efficient robust electrocatalysis. Small 19:2301468. https://doi.org/10.1002/smll.202301468

Zhang H, Wang X, Li Y, Zuo K, Lyu C (2021) A novel MnOOH coated nylon membrane for efficient removal of 2,4-dichlorophenol through peroxymonosulfate activation. J Hazard Mater 414:125526. https://doi.org/10.1016/j.jhazmat.2021.125526

Zhu L, Shi Z, Deng L (2021) Enhanced heterogeneous degradation of sulfamethoxazole via peroxymonosulfate activation with novel magnetic $MnFe_2O_4$/GCNS nanocomposite. Colloid Surface A 621:126531. https://doi.org/10.1016/j.colsurfa.2021.126531

Zou L, Xiao X, Chu C, Chen B (2021) Facile synthesis of porous $CoFe_2O_4$/graphene aerogel for catalyzing efficient removal of organic pollutants. Sci Total Environ 775:143398. https://doi.org/10.1016/j.scitotenv.2020.143398

Publisher's Note Springer Nature remains neutral with regard to jurisdictional claims in published maps and institutional affiliations.

Springer Nature or its licensor (e.g. a society or other partner) holds exclusive rights to this article under a publishing agreement with the author(s) or other rightsholder(s); author self-archiving of the accepted manuscript version of this article is solely governed by the terms of such publishing agreement and applicable law.